

Pionic Atom Formation in Halo Nuclei by (d, ^3He) Reactions

M. Fujita, S. Hirenzaki and K. Kume

Department of Physics, Nara Women's University, Nara 630-8506, Japan

Abstract

We investigate the formation cross sections of the deeply bound pionic atoms on halo nuclei theoretically. We consider one-neutron pick-up (d, ^3He) reaction for the pionic atom formation and find that the formation rate is significantly increased by the existence of the halo neutron with long tail of the wave function. This enhancement is expected to increase the experimental feasibility for the formation of the deeply bound pionic states on β -unstable nuclei.

1 Introduction

Mesic atoms are the useful laboratories for studying the meson-baryon interactions, the meson properties in nuclear medium and the nuclear properties. Among others, pionic atoms have been long utilized for such studies [1]. The binding energies and widths of the pionic bound states are expected to provide us with the unique information of the pion-nuclear interaction [2] and of the nuclear density distributions [3, 4].

The standard method to produce pionic atoms starts with injecting slow negative pions into matter. The pions will be stopped and trapped in outermost orbits of atoms, then lose energy by emitting Auger electrons and x-rays to cascade down to deeper atomic states. However, the x-ray cascade ceases at the so called 'last orbital', where the pions are absorbed by the nucleus without going to deeper atomic states. This prevents us from studying the deep pionic states for heavy nuclei that have large overlap with nuclear density [5].

To overcome this difficulty, the recoilless mesic atom production by (d, ^3He) reaction has been proposed [6]. This method tries to directly create deeply bound pions by the nuclear reaction without cascade down of the pion from the outer most orbits. This direct method was proved to be effective and powerful for the study of far deeply bound pionic atoms [7, 8]. We can now

determine the binding energies and widths of the deepest bound states such as 1s and 2p atomic states from the energy spectra of the emitted ${}^3\text{He}$. We remark that the $(d, {}^3\text{He})$ reaction is so powerful that it may also be applied to the creation of neutral meson-nucleus bound states such as the η and ω mesic nuclei [9, 10].

On the other hand, the physics of the unstable nuclei is one of the most interesting subject in modern nuclear science. Since the successful use of a new experimental tool, namely “beams of unstable nuclei” [11, 12], the properties of nuclei far from the stability line have been studied extensively in many laboratories where secondary beams of unstable nuclei are available. One of the exciting findings was the neutron halo structure around the ${}^9\text{Li}$ core in ${}^{11}\text{Li}$ [11]. Since then, the structure and reactions of β -unstable nuclei have been studied extensively both theoretically and experimentally [13, 14].

Since the repulsive S-wave pion-nucleus interaction causes the formation of the pionic halo around the core nucleus [5], the binding energies and widths of deeply bound pionic atoms are expected to be very sensitive to the structure of the nuclear surface, in particular, to the neutron skin [4]. Hence, we can expect to obtain new information on neutron/proton distribution of the unstable nuclei by observing the deeply bound pionic atoms. The determination of the neutron distributions for unstable nuclei is one of the most important subjects in the β -unstable nuclear physics [13]. In addition the $(d, {}^3\text{He})$ reaction with pionic atom formation proceeds through the single-neutron pick up and are known to be very sensitive to the single-particle properties of the neutron in nucleus [15]. Hence, we can also expect to obtain the new information of the neutron single-particle states (nlj) in unstable nuclei. This is very interesting in the context of the possible change of the magic numbers far from stability line [16].

For the formation of the deeply bound pionic atoms on unstable nuclei, we use the inverse kinematics technique, in which a light target such as deuteron is bombarded by radioactive ion (RI) beam of intermediate energy and the recoiling light ejectile ${}^3\text{He}$ is detected after forming pionic atoms in the heavy projectile [17]. We evaluate the formation cross sections for inverse kinematics reactions $d(\text{RI}, {}^3\text{He})\text{X}$ in order to examine the experimental feasibility [18]. Recently, the existence of the halo like structure of neutron distribution is predicted theoretically in medium heavy mass nuclei like Zr isotopes [19], which was not considered in our previous work [18]. This is very interesting since the existence of the long tail of the neutron wave function may enhance the formation cross section of the deeply bound pionic atoms in unstable nuclei and increase much the experimental feasibility in very unstable region of nuclear chart using the next generation of accelerators such as RIKEN RIB factory.

In this paper we study the formation cross sections of the deeply bound pionic states for the medium and heavy halo nuclei. We simulate the halo-like

structure by using the solutions of the Schrödinger equation with an one-body neutron potential for various potential depths, and we investigate the effects of the long-tail of the neutron wave functions to the (d, ^3He) spectra. In section 2, we describe our theoretical formalism. We show the numerical results in section 3. Section 4 is devoted to the summary.

2 Formalism

In this section, we describe our theoretical formalism to investigate the pionic atom formation spectra on halo nuclei. As we will describe below, we introduce a single free parameter F , a reduction factor for neutron potential depth, and simulate the halo structure by changing the parameter F . Nuclear properties, such as neutron wave functions, density distribution and one-neutron separation energies, are obtained consistently for various F values. Pionic atom structure and formation spectra are also calculated consistently for several F values. The factor F is the only free parameter introduced in the present work.

In order to simulate the halo wave functions for neutron, we solve the one-body Schrödinger equation for all occupied single-particle states for both protons and neutrons using the potential in ref. [20]. The one-body potential for protons and neutrons are given by,

$$V(r) = V_0 \frac{1}{1 + \exp((r - R_0)/\alpha_0)} - \frac{\hbar^2}{2M^2c^2} \lambda_{ls} (\boldsymbol{\ell} \cdot \mathbf{s}) \frac{1}{r} \frac{d}{dr} \left(\frac{V_0}{1 + \exp((r - R_{ls})/\alpha_{ls})} \right) + V_c(r), \quad (1)$$

where V_c is the Coulomb potential of a uniform charge distribution with the radius R_c . We adopt the potential parameters which were determined so as to fit the experimental single particle energies for Pb region in ref. [20] and these are listed in Table 1.

Here, we introduce a free parameter F which is a reduction factor for neutron potential depth to simulate the halo structure as;

$$V_0 \rightarrow F \times V_0. \quad (2)$$

This factor is introduced only for the neutron potential and the potential depth for proton is not altered for all numerical calculations in the present work.

Using the proton and neutron radial wave functions $R_{nlj}^{(p/n)}(r)$, we calculate the proton and neutron density distributions by summing up the absolute square of the wave functions for all occupied states (nlj) for proton and neutron, respectively,

$$\rho_{(p/n)}(r) = \frac{1}{4\pi} \sum_{nlj} (2j+1) |R_{nlj}^{(p/n)}(r)|^2. \quad (3)$$

We calculate the density of the target nucleus ρ_A using Eq.(3), and we evaluate the final-state nuclear density ρ_{A-1} , which appears in Eq.(14), by removing one neutron in the state which has the largest contribution to the (d,³He) spectra from the ρ_A .

The pionic atom wave functions and eigen energies are obtained by solving the Klein-Gordon equation with pion-nucleus optical potential,

$$\left[-\nabla^2 + \mu^2 + 2\mu V_{opt}(r)\right] \phi_\pi(\mathbf{r}) = [E - V_{Coul}(r)]^2 \phi_\pi(\mathbf{r}), \quad (4)$$

where μ is the reduced mass of pion-nucleus system and $V_{Coul}(r)$ is the Coulomb potential with a finite nuclear charge distribution $\rho_p(r)$ given by,

$$V_{Coul}(r) = -e^2 \int \frac{\rho_p(r')}{|\mathbf{r} - \mathbf{r}'|} d^3r'. \quad (5)$$

We use the proton and neutron density distributions ρ_p and ρ_n of target nucleus given in Eq. (3) for all densities in the Klein-Gordon equation. Hence, all nuclear densities and the pion wave function depend on the parameter F .

For the pion-nucleus optical potential, we adopt the conventional Ericson-Ericson form [21];

$$2\mu V_{opt}(r) = -4\pi \left[b(r) + \epsilon_2 B_0 \rho^2(r) \right] + 4\pi \nabla \cdot \left[c(r) + \epsilon_2^{-1} C_0 \rho^2(r) \right] L(r) \nabla, \quad (6)$$

with

$$b(r) = \epsilon_1 [b_0 \rho(r) + b_1 [\rho_n(r) - \rho_p(r)]], \quad (7)$$

$$c(r) = \epsilon_1^{-1} [c_0 \rho(r) + c_1 [\rho_n(r) - \rho_p(r)]], \quad (8)$$

$$L(r) = \left[1 + \frac{4}{3} \pi \lambda [c(r) + \epsilon_2^{-1} C_0 \rho^2(r)] \right]^{-1}. \quad (9)$$

We adopt a parameter set determined by Seki and Masutani in ref. [22] as the standard one and these are listed in Table 2.

To evaluate the formation rate of the pionic atoms in the (d,³He) reactions, we use the effective number approach [15] which is known to predict the experimental cross sections reasonably well [7]. The (d,³He) spectrum is given as;

$$\left(\frac{d^2\sigma}{d\Omega_{He} dE_{He}} \right)_{dA \rightarrow {}^3\text{He}(A-1)\pi} = \sum_{[l_\pi \otimes j_n^{-1}]} \left(\frac{d\sigma}{d\Omega} \right)_{dn \rightarrow {}^3\text{He}\pi} N_{\text{eff}} \frac{\Gamma_{\pi a}}{2\pi} \frac{1}{\Delta E^2 + \Gamma_{\pi a}^2/4}, \quad (10)$$

with

$$\Delta E = Q + m_\pi - BE_\pi + S_n - [M_d + M_n - M_{\text{He}}], \quad (11)$$

where BE_π and $\Gamma_{\pi a}$ are the binding energy and the width of pionic atom, and S_n is the neutron separation energy. These quantities also depend on the factor F introduced in Eq.(2).

The effective number N_{eff} in Eq.(10) is defined with the neutron and the pion wave functions $\psi_n(\mathbf{r})$ and $\phi_\pi(\mathbf{r})$ as,

$$N_{\text{eff}} = \sum_{JM} \left| \int \chi_f^*(\mathbf{r}) [\phi_\pi^*(\mathbf{r}) \otimes \psi_n(\mathbf{r})]_{JM} \chi_i(\mathbf{r}) d^3\mathbf{r} \right|^2, \quad (12)$$

where the deuteron and ${}^3\text{He}$ wave functions are expressed as χ_i and χ_f , and are calculated in Eikonal approximation as;

$$\chi_f^*(\mathbf{r}) \chi_i(\mathbf{r}) = \exp(i\mathbf{q} \cdot \mathbf{r}) D(z, \mathbf{b}). \quad (13)$$

The distortion factor $D(z, \mathbf{b})$ appeared in Eq. (13) is defined as;

$$D(z, \mathbf{b}) = \exp \left[-\frac{1}{2} \sigma_{dN} \int_{-\infty}^z dz' \rho_A(z', \mathbf{b}) - \frac{1}{2} \sigma_{hN} \int_z^\infty dz' \rho_{A-1}(z', \mathbf{b}) \right], \quad (14)$$

where the nuclear densities are given in Eq. (3).

We like to mention here again that we have only a single free parameter F in this model and all physical quantities are obtained in a consistent manner for each F value to simulate the effects of the halo structure on the pionic atom formation (d, ${}^3\text{He}$) spectra.

	$V_0(\text{MeV})$	$R_0(\text{fm})$	$\alpha_0(\text{fm})$	λ_{ls}	$R_{ls}(\text{fm})$	$\alpha_{ls}(\text{fm})$	$R_c(\text{fm})$
protons	-60.94	7.52	0.79	22.33	7.28	0.59	6.70
neutrons	-49.40	7.05	0.66	21.47	6.78	0.24	

Table 1: Parameters for proton and neutron one-body potential obtained in ref. [20] for Pb region.

3 Numerical results

In this section we show the numerical results for the pionic atom formation spectra in (d, ${}^3\text{He}$) reaction by varying the parameter F to simulate the halo-like structure. First, we consider the pionic atoms on ${}^{208}\text{Pb}$. The calculated neutron binding energies are listed in Table 3. Obviously, the binding energies are smaller for smaller F values. The $1i_{13/2}$ state does not bound for the

$b_0 = -0.0283m_\pi^{-1}$	$b_1 = -0.12m_\pi^{-1}$
$c_0 = 0.223m_\pi^{-3}$	$c_1 = 0.25m_\pi^{-3}$
$B_0 = 0.042 i m_\pi^{-4}$	$C_0 = 0.10 i m_\pi^{-6}$
$\lambda = 1.0$	

Table 2: Pion-nucleus potential parameters obtained in ref. [22].

values F smaller than 0.765. Thus, we vary the F between 1 and 0.765. These binding energies are used as the neutron separation energies S_n appeared in Eq.(11).

We show the nuclear density distributions in Fig. 1 for the values $F = 1.0$ and 0.765. We can see that the neutron density distribution is affected significantly by the choice of F value and has longer tail for $F=0.765$. The nuclear densities shown in Fig. 1 are used to calculate the pionic wave functions.

The density distribution of the neutron $3p_{1/2}$ state and that of the pionic 1s state are shown in Fig. 2. We can see that the neutron single-particle density in the valence level is sensitive to the F value and has halo-like tail for the smaller F values. On the other hand, the density of the pionic atom depends on the F value in rather mild manner as seen in Fig. 2. The binding energy of the 1s pionic state is 6.93MeV for $F=1$ while 6.67MeV for $F=0.765$, respectively.

We also show the calculated root mean square radii for valence neutron levels and show the dependence on the F value in Table 4. We can see that the neutron states with lower angular momenta are more sensitive to the F value and develop the longer tail. This feature is interpreted as the consequence of the centrifugal barrier and was suggested in ref. [23]. We expect that the long tail of the neutron distribution leads to larger cross section for producing deeply bound pionic states since the quasi-substitutional states are known to be largely populated for the recoilless (d, ^3He) reactions [6].

To see this, we show the calculated (d, ^3He) spectra for ^{208}Pb target in Fig. 3 as a function of Q-value. Here, we only evaluate the contributions from bound pionic states. As can be seen in the figure, we find that the formation cross section is significantly enhanced for the case of halo-like neutron distribution corresponding to $F=0.765$.

The formation cross section of $[(2p_{3/2})_n^{-1} \otimes (2p)_\pi]$ configuration, which has the largest contribution to the spectra, is around factor 3.5 larger for $F=0.765$ than that for $F=1.0$ which corresponds to no-halo case. We also find that the shape of the spectrum is considerably influenced with the change of the F value. This is due to (1) the change of the separation energy of each neutron state as shown in the Table 3, and (2) the change of the momentum transfer for different Q-values. Thus, for example, we can see from

Fig. 3 that the energy difference between two peaks $[(2p_{3/2})_n^{-1} \otimes (2p)_\pi]$ and $[(2p_{1/2})_n^{-1} \otimes (2p)_\pi]$ are much closer for $F=0.765$ case and there appears the extra strength around $Q=-127 \sim -128$ MeV due to the $[(2p_{3/2})_n^{-1} \otimes (1s)_\pi]$ and $[(2p_{1/2})_n^{-1} \otimes (1s)_\pi]$ contributions, which are negligible for $F=1.0$ case because of the smaller momentum transfer.

We also investigate the case of Xe, which is known to have large formation cross section for pionic 1s state coupled to the $s_{1/2}$ neutron state [15]. For this case, we used the radius parameters, R_0 , R_{ls} and R_c , for the proton and neutron potential listed in Table 1 by assuming the mass number dependence $A^{1/3}$. The other parameters are assumed to be the same. We show the calculated binding energies in Table 5. We do not have the bound $1h_{11/2}$ state for the value of F smaller than 0.775. The calculated root mean square radii are shown in Table 6. We find again that the long halo-like tail is developed well for $3s_{1/2}$ state, the state with the lowest angular momentum, as in the case of Pb.

We show the calculated spectra for the case of Xe target in Fig. 4 as a function of the reaction Q-value. We can see again that there exists large enhancement of the cross section for halo-like neutron states. We also find the change of the spectrum as in the case of Pb. The formation cross sections of $[(3s_{1/2})_n^{-1} \otimes (1s)_\pi]$ configuration, which has the largest contribution to the spectra, is around factor 2.9 larger for $F=0.775$ than that for $F=1.0$ which corresponds to no-halo case.

Finally, we examined the sensitivity of our results to the theoretical inputs. In Fig. 5, we show the $(d, {}^3\text{He})$ spectra for Pb which are calculated by using the nuclear density with the relativistic mean field model(RMF) [24] and with the pion-nucleus optical potential obtained by Konijn et al. [25]. The RMF model gives the nuclear density without the halo-like structure. For comparison, we also show the results calculated by the nuclear density with the potential parameters in Table 1 denoted as ρ_{speth} [20] and/or the results with the pion-nucleus optical potential by Seki and Masutani [22] (SM). As seen, the calculated spectra are slightly modified by the above choice of the nuclear densities and the pion-nucleus optical potential. But these modifications are not significant for the cases considered here. Next, in Fig. 6, we show the results by assuming the halo-like nuclear densities. We adopted the same procedure as in Section 2 to simulate the possible halo-like structure of the nuclear density. The strength of the single-nucleon potential is varied by introducing a single free parameter F as in Eq.(2). The nucleon single-particle potential by Koura (set OB) [26] is adopted to see the dependence on the nucleon-nucleus potential. For this potential, we found $F=0.715$ is the smallest F value which gives the bound $1i_{13/2}$ single-particle state. Since the overlap of the pion wave function and the nuclear density is larger for this case, we obtained significantly larger widths for the deeply bound pionic states. Thus, the calculated spectrum with the nuclear density by the single

nucleon potential by Koura is influenced as seen in Fig. 6: (i) the largest two peaks due to $[(2p_{3/2})_n^{-1} \otimes (2p)_\pi]$ and $[(2p_{1/2})_n^{-1} \otimes (2p)_\pi]$ configurations can not be distinguished, and (ii) the bump at $Q=-127 \sim -128\text{MeV}$ due to pionic 1s-states contribution is not seen with the nuclear density by Koura. However, we can see that the absolute heights of the peaks in the spectra are roughly the same. We can conclude that, though the detailed shape of the spectrum is influenced by the theoretical inputs, the formation cross section of the deeply bound pionic states is largely enhanced by the existence of the halo-like structure in the target nucleus.

B.E.(keV)	$3p_{1/2}$	$2f_{5/2}$	$3p_{3/2}$	$1i_{13/2}$	$2f_{7/2}$	$1h_{9/2}$
$F=1.0$	7761.6	8386.0	8807.6	8895.0	11252.3	11868.5
$F=0.765$	1094.4	933.91	1513.8	18.281	2787.6	2864.4

Table 3: Calculated neutron binding energies for each valence neutron level of Pb in unit of keV for $F=1.0$ and 0.765 .

$\langle r^2 \rangle^{1/2}(\text{fm})$	$3p_{1/2}$	$2f_{5/2}$	$3p_{3/2}$	$1i_{13/2}$	$2f_{7/2}$	$1h_{9/2}$
$F=1.0$	5.9145	5.7722	5.7723	6.2341	5.6795	5.6008
$F=0.765$	7.9384	6.9139	7.4099	6.5740	6.3475	5.9810

Table 4: Calculated root mean square radii for each valence neutron state of Pb in unit of fm for $F=1.0$ and 0.765 .

B.E.(keV)	$1h_{11/2}$	$3s_{1/2}$	$2d_{3/2}$	$1g_{7/2}$	$2d_{5/2}$
$F=1.0$	8215.9	9668.8	9219.1	11836.0	11726.4
$F=0.775$	121.0	2821.6	2306.4	3579.1	3946.9

Table 5: Calculated neutron binding energies for each valence neutron level of Xe in unit of keV for $F=1.0$ and 0.775 .

4 Conclusions

In this paper, we have studied theoretically the formation cross sections of the deeply bound pionic states in $(d, {}^3\text{He})$ reactions for halo nuclei. To simulate the halo-like structure of neutrons, we have simply modified the depth of the neutron potential by introducing a single free parameter F and generated the

$\langle r^2 \rangle^{1/2}(\text{fm})$	$1h_{11/2}$	$3s_{1/2}$	$2d_{3/2}$	$1g_{7/2}$	$2d_{5/2}$
$F=1.0$	5.4817	5.1079	5.0575	4.8649	4.9911
$F=0.775$	5.8531	6.2414	6.0258	5.2500	5.614

Table 6: Calculated root mean square radii for each valence neutron state of Xe in unit of fm for $F=1.0$ and 0.775 .

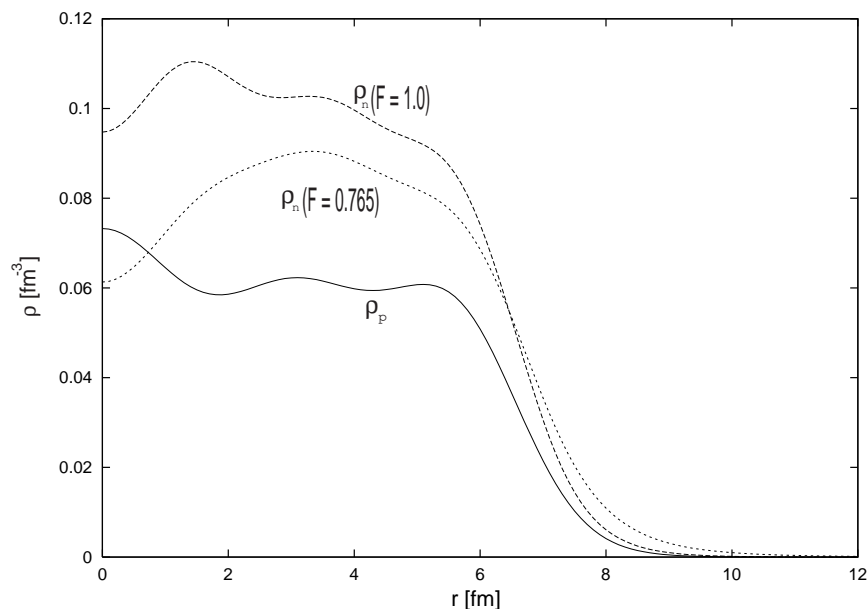


Figure 1: Neutron density distributions ρ_n are plotted as a function of the radial coordinate r for $F=1.0$ and 0.765 . Proton density ρ_p is also plotted as the solid line.

shallow neutron states with long tail. Using the neutron wave function and the nuclear densities thus obtained, we have calculated the formation cross section of the deeply bound pionic states in $(d, {}^3\text{He})$ reactions. By varying the parameter F , we can see the effect of valence neutron states on the formation spectra. We found that the formation cross section is significantly enhanced for the case with neutron halo-like states. We have examined the several theoretical models and found that the enhancement of the reaction strength due to the halo-like structure in the target nucleus is the common feature of the spectrum. For the cases with halo-like states, the reaction strengths are enhanced about a factor 3.5 for Pb and about 2.9 for Xe than the case without neutron halo. We also found that the shape of the reaction spectra is considerably affected by the choice of the strength parameter F for the

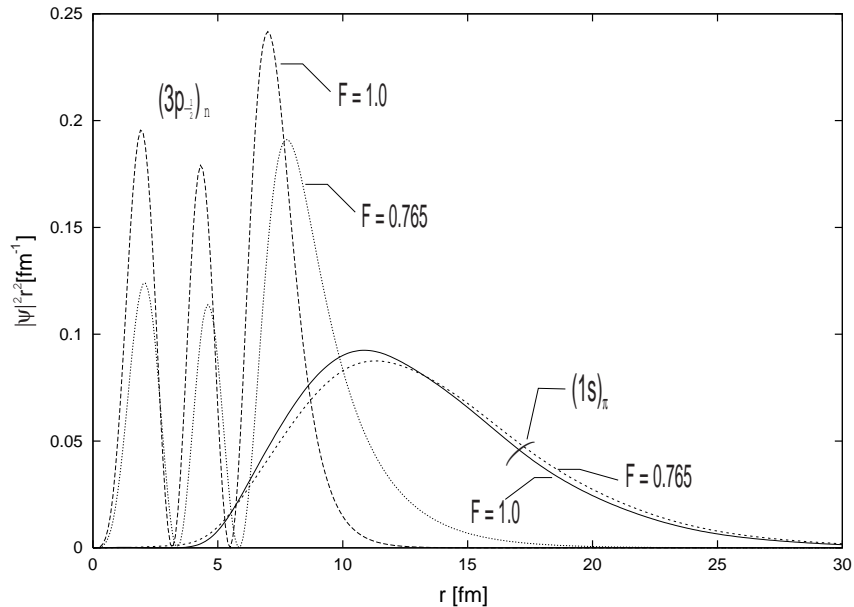


Figure 2: Density distributions of the neutron $3p_{1/2}$ and the pionic $1s$ states are shown for $F=1.0$ and 0.765 for Pb.

nucleon-nucleus potential.

We believe that the present results are relevant to the development of spectroscopic studies for the deeply bound pionic states in wide area in nuclear chart including the neutron-rich unstable nuclei.

Acknowledgments

One of us (M.F.) thanks Dr.H. Nagahiro for valuable comments. This work is partly supported by the Grants-in-Aid for Scientific Research of the Japan Ministry of Education, Culture, Sports, Science and Technology (No. 11694082 and No. 14540268).

References

- [1] T. Ericson and W. Weise, "Pions in Nuclei" (Clarendon Press, Oxford, 1988).
- [2] C. T. A. M. de Laat et al., Nucl. Phys. A523, 453 (1991).
- [3] S. Hirenzaki, T. Kajino, K.-I. Kubo, H. Toki, and I. Tanihata, Phys. Lett. **B194**, 20 (1987).

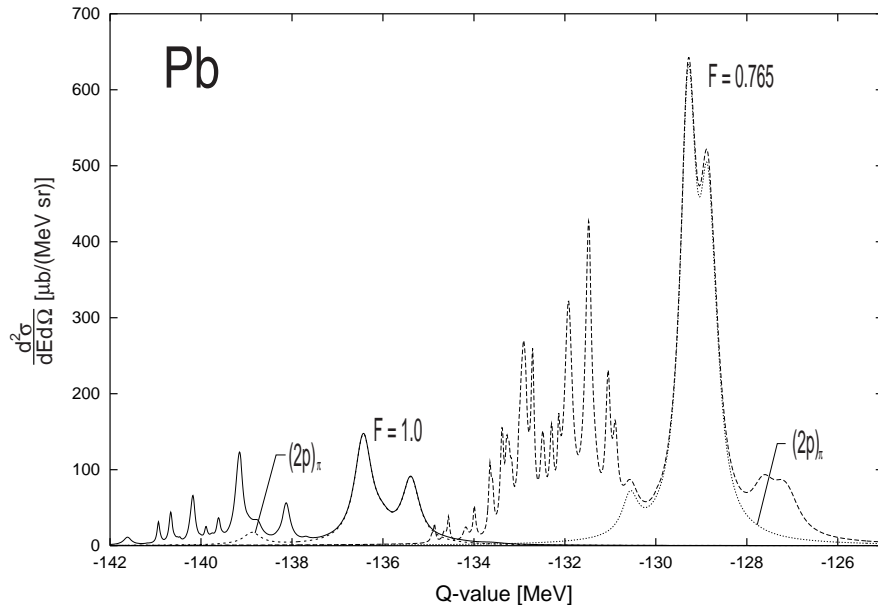


Figure 3: Formation cross sections of the bound pionic states in $(d, {}^3\text{He})$ reaction are plotted as a function of Q-value at the incident energy $T_d=500$ MeV on Pb. The solid and the dashed curves are the results with $F=1.0$ and 0.765 , respectively. The largest peak corresponds to the pionic $2p$ state, and then we show the separate contributions coming from the pionic $2p$ components as dotted curves. Instrumental energy resolution is assumed to be 50 keV.

- [4] H. Toki, S. Hirenzaki, and T. Yamazaki, Phys. Lett. **B249**, 391 (1990).
- [5] H. Toki and T. Yamazaki, Phys. Lett. **B213**, 129 (1988). H. Toki, S. Hirenzaki, T. Yamazaki, and R.S. Hayano, Nucl. Phys. **A501**, 653 (1989).
- [6] H. Toki, S. Hirenzaki, and T. Yamazaki, Nucl. Phys. **A530**, 679 (1991). S. Hirenzaki, H. Toki, and T. Yamazaki, Phys. Rev. **C44**, 2472 (1991).
- [7] T. Yamazaki *et al.*, Z. Phys. **A355**, 219 (1996), Phys. Lett. **B418**, 246 (1998). H. Gilg *et al.* Phys. Rev. **C62**, 025201 (2000). K. Itahashi *et al.*, Phys. Rev. **C62**, 025202 (2000).
- [8] A. Gillitzer *et al.*, Nucl. Phys. **A663/A664**, 206c (2000), H. Geissel *et al.*, Phys. Rev. Lett. **88**, 122301 (2002).
- [9] R. S. Hayano, S. Hirenzaki, and A. Gillitzer, Euro. Phys. J. **A6**, 99 (1999). K. Tsushima, D. H. Lu, A. W. Thomas, and K. Saito, Phys. Lett. **B443**, 26 (1998). F. Klingl, T. Waas, and W. Weise, Nucl. Phys. **A650**, 299 (1999).

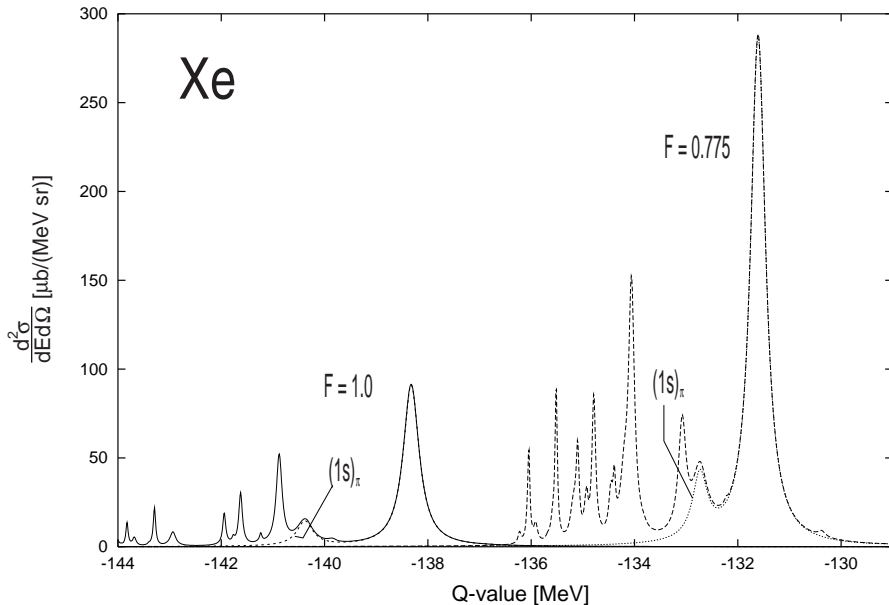


Figure 4: Formation cross sections of the bound pionic states in $(d, {}^3\text{He})$ reaction are plotted as a function of Q-value at the incident energy $T_d=500$ MeV on Xe. The solid and the dashed curves are the results with $F=1.0$ and 0.775 respectively. The largest peak corresponds to the pionic $1s$ state, and then we show the separate contributions coming from the pionic $1s$ components as dotted curves. Instrumental energy resolution is assumed to be 50 keV.

- [10] S. Hirenzaki, H. Nagahiro, T. Hatsuda, and T. Kunihiro, Nucl. Phys. A710, 131 (2002). D. Jido, H. Nagahiro, and S. Hirenzaki, Phys. Rev. C66, 045202 (2002).
- [11] I. Tanihata *et al.*, Phys. Rev. Lett. **55**, 2676 (1985).
- [12] I. Tanihata, Treatise on heavy-ion science, vol. 8, ed. D. A. Bromley (Plenum, New York, 1989) p. 443.
- [13] I. Tanihata, J. Phys. **G22**, 157 (1996).
- [14] Prog. Theor. Phys. Suppl. 142 (2001), Physics of Unstable Nuclei, eds. H. Horiuchi, T. Otsuka, and Y. Suzuki.
- [15] Y. Umemoto, S. Hirenzaki, K. Kume, and H. Toki, Prog. Theor. Phys. **103**, 337 (2000).
- [16] J. Meng, I. Tanihata, and S. Yamaji, Phys. Lett. **B419**, 1 (1998).

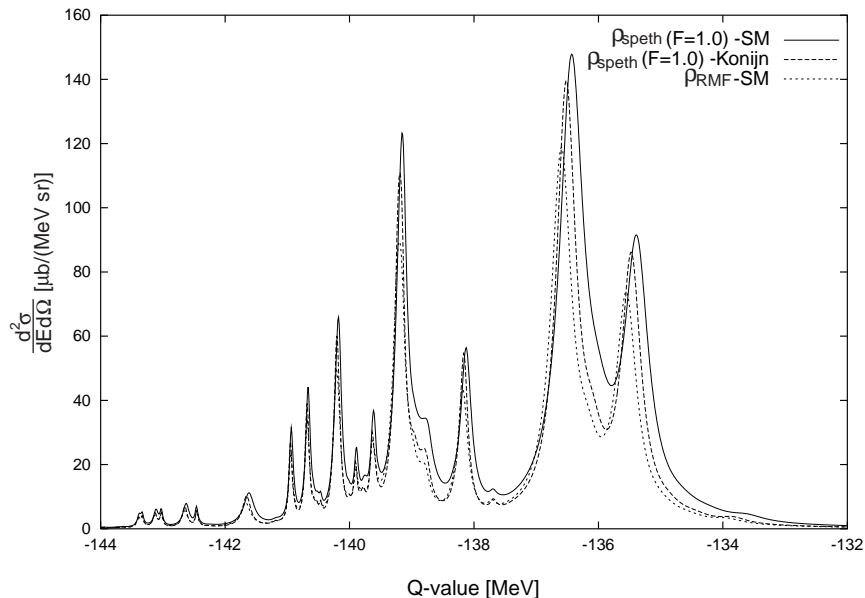


Figure 5: Formation cross sections of the bound pionic states in $(d, {}^3\text{He})$ reaction are plotted as a function of Q-value at the incident energy $T_d=500$ MeV on Pb. Each line shows the calculated spectra with the different combination of the nuclear density and the pion-nucleus optical potential as indicated in the figure. All densities do not have the halo structure. Solid line indicates the same result as the solid line in Fig. 3. Instrumental energy resolution is assumed to be 50 keV. See text for the detail.

- [17] T. Yamazaki, R. S. Hayano, H. Toki, and P. Kienle, Nucl. Instrum. Methods **A292**, 619 (1990); T. Yamazaki, R. S. Hayano, and H. Toki, Nucl. Inst. Meth. Phys. Res. **A305**, 406 (1991).
- [18] Y. Umemoto, S. Hirenzaki, K. Kume, H. Toki, and I. Tanihata, Nucl. Phys. A679, 549 (2001).
- [19] J. Meng and P. Ring, Phys. Rev. Lett. 80, 460 (1998).
- [20] J. Speth, E. Werner, and W. Wild, Phys. Rep. **33**, 127 (1977).
- [21] M. Ericson and T. E. O. Ericson, Ann. of Phys. 36, 496 (1966).
- [22] R. Seki and K. Masutani, Phys.Rev. **C27**, 2799 (1983).
- [23] I. Tanihata, D. Hirata, and H. Toki, Nucl. Phys. A583, 769 (1995).
- [24] D. Hirata, H. Toki, T.Watabe, I.Tanihata, and B.V.Carlson, Phys. Rev. C44, 1467 (1991).

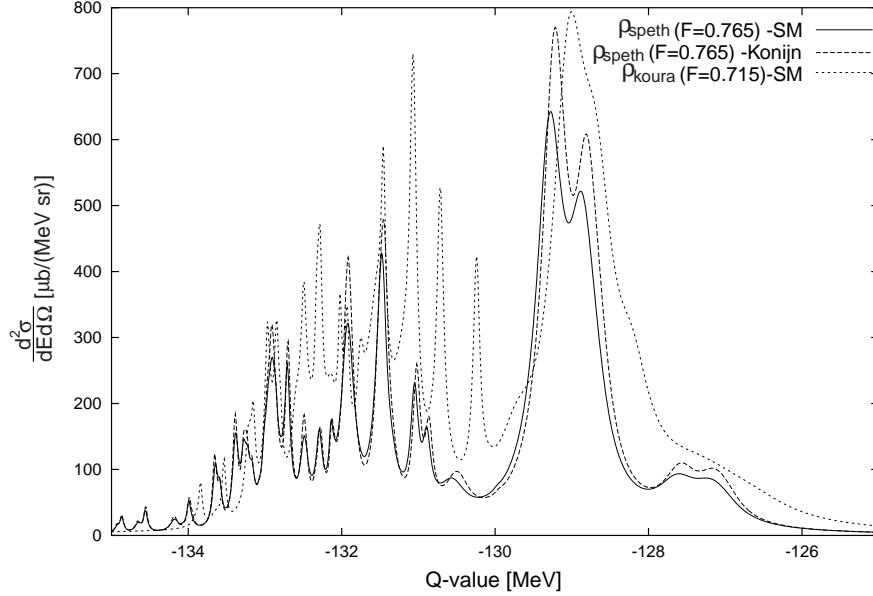


Figure 6: Formation cross sections of the bound pionic states in $(d, {}^3\text{He})$ reaction are plotted as a function of Q-value at the incident energy $T_d=500$ MeV on Pb. Each line shows the calculated spectra with the different combination of the nuclear density and the pion-nucleus optical potential as indicated in the figure. All densities are expected to simulate halo structure. Solid line indicates the same result as the dashed line in Fig. 3. Instrumental energy resolution is assumed to be 50 keV. See text for the detail.

[25] J. Konijn, C.T.A.M. de Laat, and A. Taal, Nucl. Phys. A519, 773 (1990).

[26] H. Koura and M. Yamada, Nucl. Phys. A671, 96 (2000).